Journal of Porphyrins and Phthalocyanines
J. Porphyrins Phthalocyanines 2014; **18**: 366–379
DOI: 10.1142/S1088424614500072

Published at http://www.worldscinet.com/jpp/

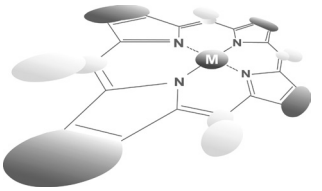

Discotic liquid crystals of transition metal complexes 50†: spiranthes-like supramolecular structure of phthalocyanine-fullerene dyads

Aya Ishikawa[a], Kenta Ono[a], Kazuchika Ohta*[a◊], Mikio Yasutake[b], Musubu Ichikawa[a] and Eiji Itoh[c]

[a] *Smart Material Science and Technology, Interdisciplinary Graduate School of Science and Technology, Shinshu University, 1-15-1 Tokida, Ueda 386-8567, Japan*
[b] *Comprehensive Analysis Center for Science, Saitama University, 255 Shimo-okubo, Sakura-ku, Saitama 338-8570, Japan*
[c] *Department of Electrical and Electronic Engineering, Shinshu University, 4-17-1 Wakasato, Nagano 380-8553, Japan*

Received 23 November 2013
Accepted 22 January 2014

ABSTRACT: We have synthesized novel liquid crystalline Pc-C_{60} dyads **$(C_nS)_6$PcCu-C_{60}** (n = 14, 16, 18: **1a–1c**) by using our developed synthetic method in order to investigate the mesomorphism and alignment behavior. Each of the **$(C_nS)_6$PcCu-C_{60}** dyads shows perfect homeotropic alignment in the Col_{ho} mesophase between two glass plates for n = 14, 16, 18 and also on a glass plate for n = 14, although none of the parent Pc compounds **$(C_nS)_8$PcCu** and the Pc precursors **$(C_nS)_6$PcCu-OH** and **$(C_nS)_6$PcCu-OFBA** shows homeotropic alignment. It may be attributed to the strong affinity between fullerene and glass surface. Although the reason is not so clear at the present time, this is very useful guideline for the molecular design to prepare homeotropic alignment-showing discotic liquid crystals. Very interestingly, the spherical C_{60} parts form a helical structure around the column formed by the disk-like Pc parts. This supramolecular structure very resembles spiranthes. The spiranthes-like supramolecular structure is compatible with one-dimensional nano-array expecting the high conversion efficiency of solar cells.

KEYWORDS: discotic liquid crystal, phthalocyanine, fullerene, dyad, homeotropic alignment, spiranthes-like supramolecular structure.

INTRODUCTION

In recent years, organic thin film solar cell is paid attention very much, because it has flexibility and easiness of film formation [1–4]. However, the conversion efficiency is still low in comparison with single crystal silicon solar cell [1]. Hence, the conversion efficiency has been raised mainly by using bulk hetero junction of donor and acceptor [1]. Recently, Yoshikawa *et al*. proposed one-dimensional (1D) nano-array structure of donor and acceptor [5] illustrated in Fig. 1a. If this structure would be realized, we could develop organic thin film solar cell showing much higher conversion efficiency [5]. However, no method has been developed to obtain such an advantageous 1D nano-array structure in an easy way.

On the other hand, liquid crystalline donor–acceptor (D–A) complexes may display superb performance in organic thin film solar cells [6–30]. They can greatly reduce their costs to manufacture the solar cells. Especially, columnar mesophases in homeotropic alignment are so favorable to obtain higher photoelectric conversion efficiency which can be attributable to larger π–π stacking of the π-conjugated macrocycles [24]. In 2001, we found at the first time that phthalocyanine (Pc)-based discotic liquid

◊SPP full member in good standing

*Correspondence to: Kazuchika Ohta, email: ko52517@shinshu-u.ac.jp, tel/fax: +81 268-21-5492

†Part 49: reference 13 in this paper

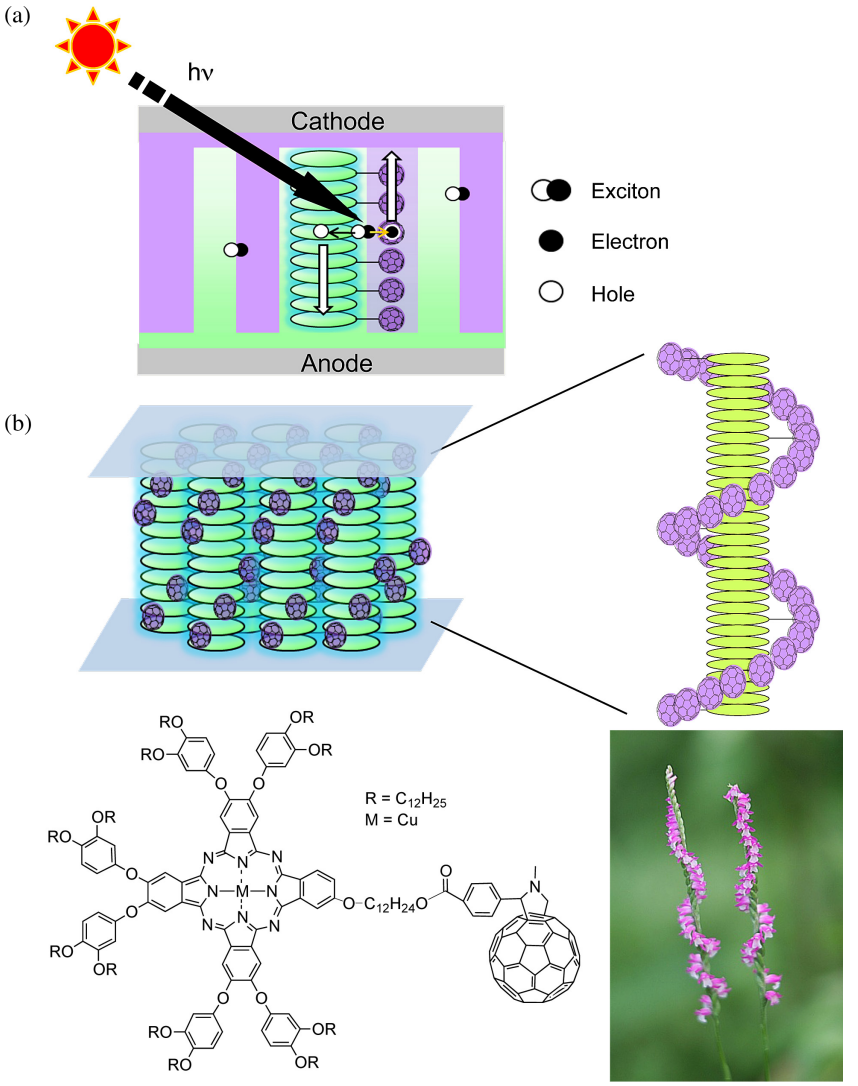

Fig. 1. Resemblance between (a) 1D nano-array structure proposed by Yoshikawa *et al.* [5] and (b) homeotropic alignment with spiranthes-like supramolecular structure of liquid crystalline Pc-C_{60} dyad found by us [36]

crystalline compounds, **[(C_nO)$_2$PhO]$_8$PcCu** (n = 11~14), spontaneously show perfect homeotropic alignment between two glass plates for the tetragonal columnar (Col_{tet}) mesophase [31–34]. Furthermore, in 2007 we reported the first liquid crystalline phthalocyanine-fullerene dyad, **PcCu(OMalC_{60}) (OCH_3)**, exhibiting perfect homeotropic alignment in the hexagonal columnar phase (Col_h) at high temperatures [19]. Since then, the other groups also reported liquid crystalline phthalocyanine-fullerene dyads [23,25,29], and we further found that several kinds of new homeotropic alignment-showing liquid crystalline phthalocyanine-fullerene (Pc-C_{60}) dyads [28, 30, 35, 36] which were derived from the perfect homeotropic alignment-showing parent Pc compound, **[(C_nO)$_2$PhO]$_8$PcCu**. Figure 1b illustrates a molecular structure and a schematic model of the homeotropic alignment for a representative example of **[($C_{12}O$)$_2$PhO]$_6$PcCu-C_{60}** [36]. It was established at the first time by using our developed two X-ray diffraction methods in our previous work [36] that the disk-like Pc parts pile up to form columns, which are aligned homeotropically between two glass plates, and the spherical C_{60} parts pile up helically around the Pc columns. This supramolecular structure very resembles spiranthes [37]. The spiranthes-like supramolecular structure of the Pc-C_{60} dyad is compatible with the 1D nano-array of donor and acceptor mentioned above. Therefore, these Pc-C_{60} dyads may be the most suitable material candidates for organic thin film solar cell. However, each of the homeotropic alignment-showing dyads, **[(C_nO)$_2$PhO]$_6$PcCu-C_{60}** [36], was obtained only from the homeotropic alignment-showing parent Pc compound, **[(C_nO)$_2$PhO]$_8$PcCu** [31], as illustrated in Fig. 2a. The synthesis of the starting materials of phthalonitriles was long and time consuming [31, 34]. It remained as a big problem for the application to solar cell. On the other hand, the starting materials of phthalonitriles for the alkylthio-substituted Pc compounds, **(C_nS)$_8$PcCu**, could be easily prepared in shorter synthetic route, but the **(C_nS)$_8$PcCu** derivatives do not show homeotropic

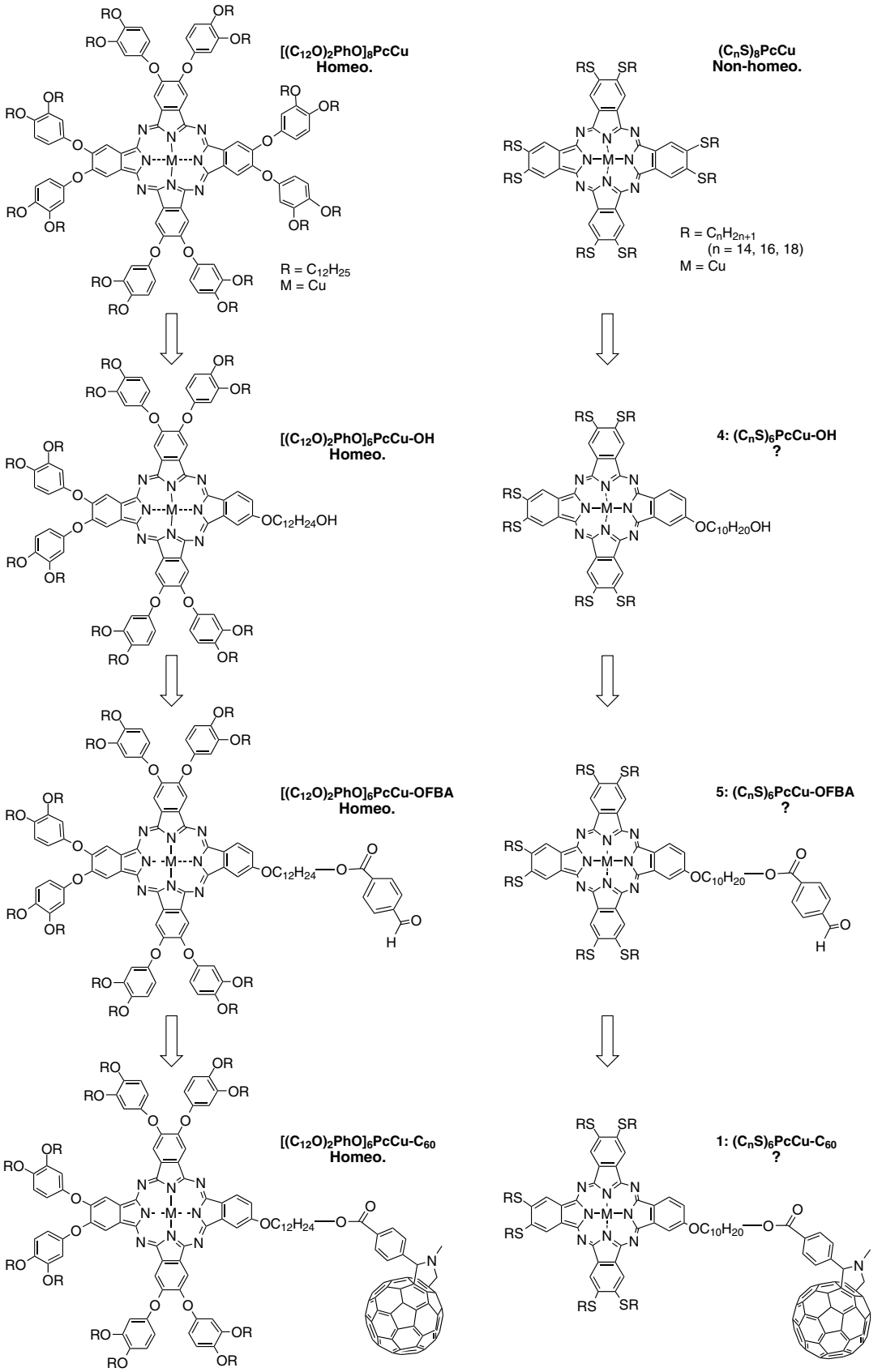

(a) Previous work (b) This work

Fig. 2. Purpose of this work. Can one obtain novel Pc-C_{60} dyads showing homeotripic alignment from their non-homeotropic parent Pc derivatives?

alignment [38]. However, it was very interesting for us to investigate whether we would be able to obtain novel homeotropic alignment-showing Pc-C_{60} dyads from the corresponding non-homeotropic alignment-showing parent Pc compound. Therefore, in this work we have synthesized the present Pc-C_{60} dyads **$(C_nS)_6$PcCu-C_{60}** (n = 14, 16, 18) from the non-homeotropic alignment-showing parent Pc compounds **$(C_nS)_8$PcCu** *via* the precursors **$(C_nS)_6$PcCu-OH** and **$(C_nS)_6$PcCu-OFBA**, in order to investigate their mesomorphism and alignment behavior, as illustrated in Fig. 2b.

Very interestingly, each of the **$(C_nS)_6$PcCu-C_{60}** (n = 14, 16, 18) dyads synthesized in this work shows perfect homeotropic alignment similarly to the previous **$[(C_nO)_2PhO]_6$PcCu-C_{60}** dyads, although neither the parent **$(C_nS)_8$PcCu** compounds nor the precursors **$(C_nS)_6$PcCu-OFBA** and **$(C_nS)_6$PcCu-OH** show homeotropic alignment. Furthermore, the C_{60} moieties form a helical structure around the column formed by the Pc disks. This supramolecular structure very resembles spiranthes. The spiranthes-like supramolecular structure is compatible with one-dimensional nano-array expecting the high conversion efficiency of solar cells. We wish to report here the synthesis and interesting mesomorphism with spiranthes-like supramolecular structure of the novel liquid crystalline **$(C_nS)_6$PcCu-C_{60}** dyads.

EXPERIMENTAL

Synthesis

The final target Pc-C_{60} dyads, **$(C_nS)_6$PcCu-C_{60}** [**1a–1c**: n = 14(**a**), 16(**b**), 18(**c**)], were synthesized according to Scheme 1. The phthalonitriles, **2** and **3a–3c**, were prepared by the methods of Serin *et al.* [39] and Wöhrle *et al*. [40], respectively. The Pc precursors, **$(C_nS)_6$PcCu-OH** (**4a–4c**), were synthesized from these two different phthalonitriles **2** and **3a–3c** in a molecular ratio of 3:1. The terminal OH group in **4a–4c** was esterified with *p*-formyl benzoic acid by Steglich reaction [41] to afford **$(C_nS)_6$PcCu-OFBA** (**5a–5c**). Finally, the target Pc-C_{60} dyads, **$(C_nS)_6$PcCu-C_{60}** (**1a–5c**), were synthesized from **5a–5c** with *N*-methylglycine and fullerene by Prato reaction [42].

We describe here the detailed procedures only for the representative derivatives, **2**, **3b**, **4b**, **5b** and **1b**. The rest of the derivatives, **3a**, **3c**, **4a**, **4c**, **5a**, **5c** and **1a**, **1c**, were prepared by same procedures. The details of these compounds are described in electronic supplementary material (see Supporting information).

4-(10-hydoroxydecyloxy)phthalonitrile (2). A mixture of 4-nitrophthalonitrile (0.500 g, 2.89 mmol), dry DMA (30 mL) and 1,10-decanediol (3.01 g, 17.3 mmol)

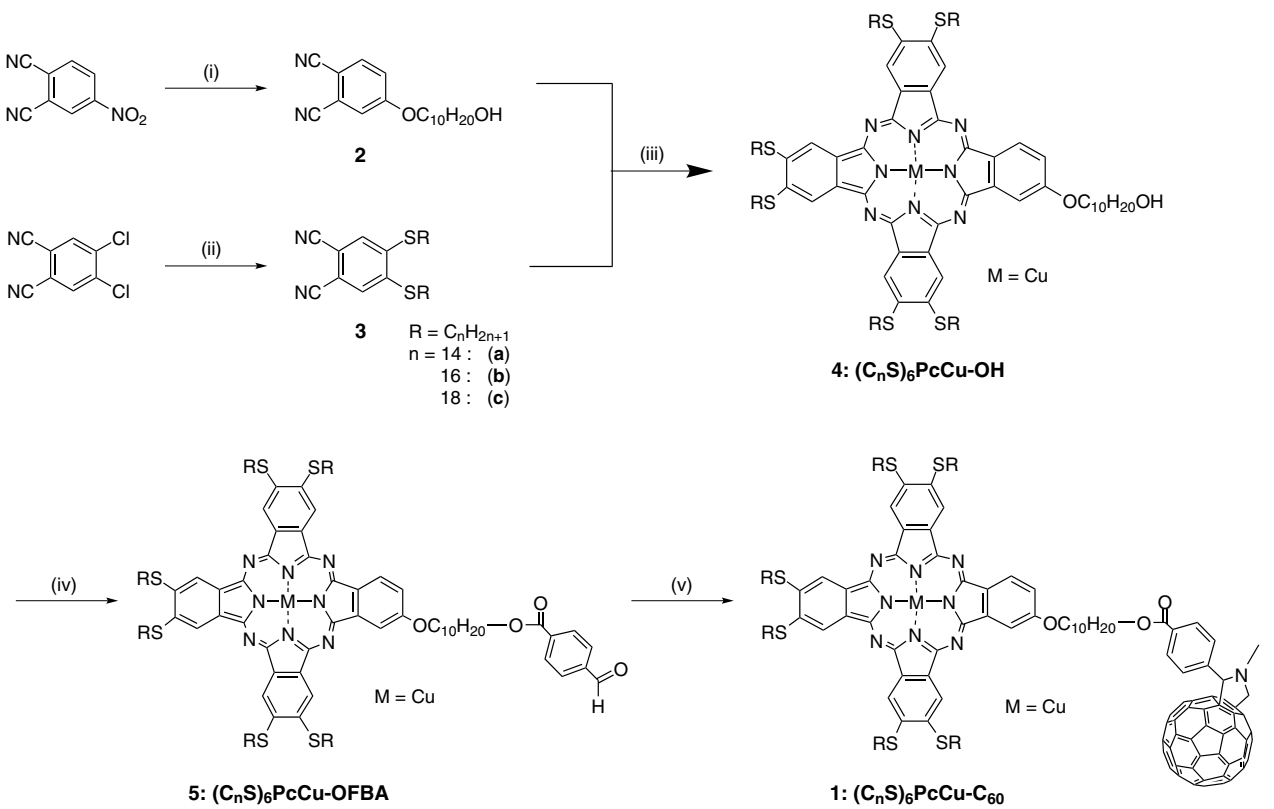

Scheme 1. Synthentic route for **$(C_nS)_6$PcCu-C_{60}** (**1a–1c**): (i) $HOC_{10}H_{20}OH$, K_2CO_3, DMAc, (ii) RSH, K_2CO_3, DMSO, (iii) $CuCl_2$, DBU, 1-hexanol, oil bath/N_2, (iv) *p*-formyl benzoic acid, DCC, DMAP, $C_2H_4Cl_2$, for n = 14; p-formyl benzoic acid, DCC, DMAP, CH_2Cl_2, for n = 16, 18, and (v) N-methylglycine, C_{60}, toluene. DMAc = *N*,*N*′-dimethylacetamide, DMSO = dimethylsulfoxide, DBU = 1,8-diazabicyclo[5,4,0]-undec-7-ene, DCC = *N*,*N*′-dicyclohexylcarbodiimide and DMAP = 4-dimethylaminopyridine

was heated at 105 °C for 0.5 h with stirring under nitrogen atmosphere. Then, potassium carbonate (2.39 g, 17.3 mmol) was added and the mixture was heated at 105 °C for 18 h with stirring under nitrogen atmosphere further. After cooling to rt, the reaction mixture was extracted with dichloromethane and washed with water. The organic layer was dried over Na_2SO_4 and evaporated in *vacuo*. The residue was purified by column chromatography (silica gel 100 g, chloroform:ethyl acetate = 3:2, R_f = 0.63). After removal of solvent, a pale yellow solid was obtained (0.501 g, yield 57.7%, mp 61.0 °C). IR (KBr): ν, cm^{-1} 3550.50 (–OH), 2927.30, 2850.87 (–CH_2–), 2227.51 (–CN), 1592.95 (C=C). ^{1}H NMR ($CDCl_3$, TMS): δ, ppm 7.70 (d, 1H, *J* = 8.8 Hz, Ar-*H*), 7.25 (d, 1H, *J* = 8.8 Hz, Ar-*H*), 7.17 (dd, 1H, J_1 = 8.8 Hz, J_2 = 2.8 Hz, Ar-*H*), 4.05 (t, 2H, *J* = 7.1, –OCH_2–), 3.67 (t, 2H, *J* = 7.3, –CH_2–), 1.89–1.81 (m, 2H, –CH_2–), 1.65~1.56 (m, 2H, –CH_2–), 1.41–1.32 (m, 12H, –CH_2–).

4,5-bis(hexadecylthio)phthalonitrile (3b). A mixture of 4,5-dichlorophthalonitrile (1.00 g, 5.08 mmol), hexadecane-1-thiol (3.17 g, 12.3 mmol), dry DMSO (20 mL) and potassium carbonate (2.76 g, 20.0 mmol) was heated at 110 °C for 1.5 h with stirring under nitrogen atmosphere. After cooling to rt, the reaction mixture was extracted with chloroform and washed with water. The organic layer was dried over Na_2SO_4 and evaporated in *vacuo*. The residue was recrystallized from *n*-hexane at -20 °C. The residue was purified by column chromatography (silica gel 50 g, chloroform, R_f = 0.69). After removal of solvent, lilac solid was obtained (2.42 g, yield 74.2%, mp 71.0 °C). IR (KBr): ν, cm^{-1} 2919.61, 2850.14 (–CH_2–), 2227.32 (–CN), 1562.96 (C=C). ^{1}H NMR ($CDCl_3$, TMS): δ, ppm 7.40 (s, 2H, Ar-*H*), 3.01 (t, 4H, *J* = 8.1 Hz, –S–CH_2–), 1.79–1.70 (m, 4H, –CH_2–), 1.26 (s, 48H, –CH_2–), 0.88 (t, 6H, *J* = 7.6, –CH_3).

$(C_{16}S)_6$PcCu-OH (4b). A mixture of 4-(10-hydroxydecyloxy)-phthalonitrile (**2**: 0.0800 g, 0.266 mmol), 4,5-bis-(hexadecylthio)-phthalonitrile (**3b**: 0.513 g, 0.800 mmol), 1-hexanol (15 mL) and $CuCl_2$ (55 mg, 0.41 mmol) was refluxed under nitrogen atmosphere for 0.5 h. Then, DBU (8 drops) was added and the mixture was refluxed under nitrogen atmosphere for 24 h. After cooling to rt, methanol was poured into the reaction mixture to precipitate the target compound. The methanolic layer was removed by filtration. The residue was washed with methanol, ethanol and acetone successively, extracted with chloroform and washed with water. The organic layer was dried over Na_2SO_4 and evaporated in *vacuo*. The crude product was purified by column chromatography (silica gel 150 g, chloroform, Rf = 0.15). After removal of solvent, dark green solid was obtained (0.171 g, yield 28.1%). Elemental analysis and MALDI-TOF mass data: see Tables 1 and 2 and Fig. S1-1. UV-vis spectral data: see Table 3 and Fig. S2. Phase transition behavior: see Table 4.

$(C_{16}S)_6$PcCu-OFBA (5b). A mixture of **$(C_{16}S)_6$PcCu-OH** (**4b**: 0.103 g, 0.0448 mmol), *p*-formyl benzoic acid (0.0246 g, 0.168 mmol), dry CH_2Cl_2 (20 mL) was refluxed under nitrogen atmosphere for 0.5 h. Then, *N*,*N*′-dicyclohexylcarbodiimide (0.0988 g, 0.479 mmol), *N*,*N*-dimethyl-4-aminopyridine (0.0337 g, 0.276 mmol) was added and the mixture was refluxed under nitrogen atmosphere for 24 h. After cooling to rt, methanol was poured into the reaction mixture to precipitate the target compound. The methanolic layer was removed by filtration. The residue was washed with methanol and hot acetone successively, extracted with chloroform and washed with water. The organic layer was dried over Na_2SO_4 and evaporated in *vacuo*. The crude product was purified by column chromatography (silica gel 80 g, chloroform, Rf = 0.78). After removal of solvent, dark green solid was obtained (0.0895 g, yield 83.0%). Elemental analysis and MALDI-TOF mass data: see Tables 1 and 2 and Fig. S1-2. UV-vis spectral data: see Table 3 and Fig. S2. Phase transition behavior: see Table 4.

$(C_{16}S)_6$PcCu-C_{60} (1b). A mixture of **$(C_{16}S)_6$PcCu-OFBA** (**5b**: 0.0548 g, 0.0227 mmol), C_{60} fullerene (0.0328 g, 0.0455 mmol), dry toluene (20 mL), *N*-methylglycine (0.0050 g, 0.056 mmol) was refluxed under nitrogen atmosphere for 14 h. After cooling to rt., the solvent was evaporated under reduced pressure. The residue extracted with chloroform and washed with water. The organic layer was dried over Na_2SO_4 and evaporated in *vacuo*. The crude product was purified by column chromatography (silica gel 80 g, chloroform:*n*-hexane = 1:1, Rf = 0.40) and further purification was carried out by using HPLC (Japan Analytical Industry Co. Ltd: LC-918). After removal of solvent, dark green solid was obtained (0.0449 g, yield 62.4%). Elemental analysis and MALDI-TOF mass data: see Tables 1 and 2 and Fig. S1-3. UV-vis spectral data: see Table 3 and Fig. S2. Phase transition behavior: see Table 4.

Measurements

The infrared absorption spectra were recorded by using a Nicolet NEXUS670 FT-IR. The ^{1}H NMR measurements were carried out by using ^{1}H NMR (Bruker Ultrashield 400 M Hz). The elemental analyses were performed by using a Perkin-Elmer Elemental Analyzer 2400. The MALDI-TOF mass spectral measurements were carried out by using a Bruker Daltonics Autoflex III spectrometer (matrix: dithranol). Electronic absorption (UV-vis) spectra were recorded by using a Hitachi U-4100 spectrophotometer. Phase transition behavior of the present compounds was observed with polarizing optical microscope (Nikon ECLIPSE E600 POL) equipped with a Mettler FP82HT hot stage and a Mettler FP-90 Central Processor, and a Shimadzu DSC-50 differential scanning calorimeter. The mesophases were identified by using a small angle X-ray diffractometer (Bruker Mac SAXS System) equipped with a temperature-variable sample holder adopted a Mettler FP82HT hot stage. Figures S3 and

S4 illustrate the setup of the SAXS system and the setup of the temperature-variable sample holder, respectively. As can be seen from Fig. S1, the generated X-ray is bent by two convergence monochrometers to produce point X-ray beam (diameter = 1.0 mm). The point beam runs through holes of the temperature-variable sample holder. As illustrated in Fig. S2, into the temperature-variable sample holder of Mettler FP82HT hot stage, a glass plate (76 mm × 19 mm × 1.0 mm) having a hole (diameter = 1.5 mm) is inserted. The hole can be charged with a powder sample (*ca.* 1 mg). The measurable range is from 3.0 Å to 100 Å and the temperature range is from rt to 375 °C. This SAXS system is available for all condensed phases including fluid nematic phase and isotropic liquid.

RESULTS AND DISCUSSION

Synthesis

Each of the phthalonitriles **2** and **3a–3c** could be easily prepared from the commercially available starting materials by one step. The yields of **3a–3c** were relatively good at 62.2~74.2%. However, the yields of the 3:1 Pc precursors, **$(C_nS)_6$PcCu-OH** (**4a–4c**), were low at 28.1~31.4% (Table 1), because the 4:0 Pc by-products were not avoided in this reaction. On the other hand, the precursors **$(C_nS)_6$PcCu-OFBA** (**5a–5c**) could be obtained in high yields at 73.8~94.0% by the esterification of Steglich reaction (Table 1). The reaction solvent was dichloromethane for the esterification of **4b**, **4c** → **5b**, **5c**, but the reaction of **4a** → **5a** did not well proceed in dichloromethane. It was attributed to the low solubility of **4a** in dichloromethane. When the reaction solvent was changed from dichloromethane (bp = 39.8 °C, ε = 9.1) to 1, 2-dichloroethane (bp = 83.5 °C, ε = 10.45), the reaction smoothly proceeded. The final target Pc-C_{60} dyads, **$(C_nS)_6$PcCu-C_{60}** (**1a–1e**), were obtained in yields of 55.3~62.4% by Prato reaction [42] (Table 1).

As can be seen from the data of MALDI-TOF mass and elemental analysis listed in Table 1, the observed values of the Pc precursors, **$(C_nS)_6$PcCu-OH** (**4a**–**4c**) and **$(C_nS)_6$PcCu-OFBA** (**5a–5c**), were in good accordance with the calculated values, so that we confirmed that they could be surely prepared. On the other hand, elemental analysis of the Pc-C_{60} dyads synthesized in our previous work was also carried out, but it was not completely burnt out that the observed carbon content showed lower percentage than the calculated value by several percent [35]. This is a well-known characteristic of less flammable phthalocyanine derivatives [43]. Hence, we did not furthermore carry out the elemental analyses for other Pc-C_{60} dyads **1a–1c** and the results of the elemental analyses are omitted here for **1a–1c**. However, as can be seen from Table 2 and Fig. S1, the observed and calculated values of exact mass, for example, those of **$(C_{16}S)_6$PcCu-C_{60}** (**1b**) are (3163.63, 2443.56) and 3163.63, respectively. The observed values gave two peaks for all the **$(C_nS)_6$PcCu-C_{60}** (**1a–1c**) dyads. One peak corresponds to the calculated exact mass. On the other hand, another peak corresponds to an exact mass smaller by 720 than the calculated exact mass. The mass of 720 is compatible with the molecular weight of fullerene (C_{60}). The fraction peak that is smaller by 720 than the calculated value may be resulted from cleavage of the fullerene (C_{60}) moiety from the **$(C_nS)_6$PcCu-C_{60}** (**1a–1c**) dyads by the laser irradiation in the MALDI-TOF mass measurements.

To further confirm the formation of these Pc-C_{60} dyads, electronic absorption spectra were measured for the chloroform solutions of the **$(C_nS)_6$PcCu-C_{60}** (**1a–1c**) dyads. The electronic spectral data are summarized in Table 3. An absorption characteristic to fullerene appears at *ca.* 250 nm in the electronic spectra [44]. As can be seem from this table, each of the **$(C_nS)_6$PcCu-C_{60}** (**1a–1c**) dyads gave an additional peak at *ca.* 250~256 nm characteristic to fullerene moiety. The **$(C_nS)_6$PcCu-OFBA** precursors did not give such an additional peak at

Table 1. Elemental analysis data and yields of **$(C_nS)_6$PcCu-OH (4a–4c)**, **$(C_nS)_6$PcCu-OFBA (5a–5c)** and **$(C_nS)_6$PcCu-C_{60} (1a–1c)**

Compound	Mol. formula (Mol. wt)	Found (Calcd.) (%)			Yield (%)
		C	H	N	
4a: $(C_{14}S)_6$PcCu-OH	$C_{126}H_{204}N_8O_2S_6Cu$ (2118.96)	71.25 (71.42)	9.78 (9.70)	5.28 (5.29)	31.4
4b: $(C_{16}S)_6$PcCu-OH	$C_{138}H_{228}N_8O_2S_6Cu$ (2287.28)	71.89 (72.47)	10.05 (10.05)	4.94 (4.90)	28.1
4c: $(C_{18}S)_6$PcCu-OH	$C_{150}H_{252}N_8O_2S_6Cu$ (2455.59)	73.25 (73.37)	10.44 (10.34)	4.66 (4.56)	29.3
5a: $(C_{14}S)_6$PcCu-OFBA	$C_{134}H_{208}N_8O_4S_6Cu$ (2251.07)	71.66 (71.50)	9.50 (9.31)	4.84 (4.98)	73.9
5b: $(C_{16}S)_6$PcCu-OFBA	$C_{146}H_{232}N_8O_4S_6Cu$ (2419.41)	72.05 (72.48)	9.60 (9.67)	4.54 (4.63)	83.0
5c: $(C_{18}S)_6$PcCu-OFBA	$C_{158}H_{256}N_8O_4S_6Cu$ (2587.71)	73.34 (73.34)	10.09 (9.97)	4.33 (4.33)	94.0
1a: $(C_{14}S)_6$PcCu-C_{60}	$C_{196}H_{213}N_9O_3S_6Cu$ (2998.76)	—	—	—	59.0
1b: $(C_{16}S)_6$PcCu-C_{60}	$C_{208}H_{237}N_9O_3S_6Cu$ (3167.16)	—	—	—	62.4
1c: $(C_{18}S)_6$PcCu-C_{60}	$C_{230}H_{261}N_9O_3S_6Cu$ (3335.43)	—	—	—	55.3

Table 2. MALDI-TOF mass spectral data of **$(C_nS)_6$PcCu-OH (4a–4c)**, **$(C_nS)_6$PcCu-OFBA (5a–5c)** and **$(C_nS)_6$PcCu-C_{60} (1a–1c)**

Compound	Exact mass (M^+) calculated	Exact mass (M^+) observed
4a: $(C_{14}S)_6$PcCu-OH	2116.37	2116.30
4b: $(C_{16}S)_6$PcCu-OH	2284.56	2284.51
4c: $(C_{18}S)_6$PcCu-OH	2452.75	2452.65
5a: $(C_{14}S)_6$PcCu-OFBA	2248.39	2248.29
5b: $(C_{16}S)_6$PcCu-OFBA	2416.58	2416.53
5c: $(C_{18}S)_6$PcCu-OFBA	2584.77	2584.43
1a: $(C_{14}S)_6$PcCu-C_{60}	2995.44 (2275.44)	2995.40 (2275.36)
1b: $(C_{16}S)_6$PcCu-C_{60}	3163.63 (2443.63)	3163.63 (2443.56)
1c: $(C_{18}S)_6$PcCu-C_{60}	3331.82 (2611.82)	3331.81 (2611.88)

Table 3. UV-vis spectral data of compounds **4**, **5** and **1** in chloroform

Compound	Concentration# (X10^{-5} mol/l)	λ_{max} (nm) (log ε)					
		C_{60} peak	Soret-band			Q-band	
						Q_{0-1} band	Q_{0-0} band
4a: $(C_{14}S)_6$PcCu-OH	1.0	—	264.1 (4.62)	325.7 (4.83)	428.3 (4.36)	635.9 (4.59)	705.0 (5.07)
4b: $(C_{14}S)_6$PcCu-OH	1.1	—	265.5 (4.68)	329.5 (4.85)	427.5 (4.42)	633.4 (4.62)	705.2 (5.10)
4c: $(C_{14}S)_6$PcCu-OH	1.0	—	264.7 (4.71)	331.1 (4.89)	427.7 (4.44)	631.6 (4.63)	705.3 (5.12)
5a: $(C_{14}S)_6$PcCu-OFBA	1.0	—	258.1 (4.74)	328.1 (4.82)	425.3 (4.36)	632.3 (4.58)	705.8 (5.09)
5b: $(C_{16}S)_6$PcCu-OFBA	0.99	—	259.1 (4.83)	332.1 (4.90)	424.5 (4.45)	633.4 (4.66)	705.2 (5.15)
5c: $(C_{18}S)_6$PcCu-OFBA	1.0	—	260.2 (4.72)	333.7 (4.77)	427.5 (4.30)	632.7 (4.52)	705.7 (5.04)
1a: $(C_{14}S)_6$PcCu-C_{60}	1.0	255.8 (5.11)	—	325.5 (4.98)	432.6 (4.38)	*ca.* 643 (4.62)	705.4 (4.96)
1b: $(C_{16}S)_6$PcCu-C_{60}	1.0	255.8 (5.19)	270.1 (sh)	322.4 (5.04)	431.7 (4.49)	*ca.* 642 (4.73)	705.2 (5.03)
1c: $(C_{18}S)_6$PcCu-C_{60}	0.99	249.6 (5.11)	—	321.5 (5.00)	427.1 (4.45)	*ca.* 646 (4.73)	704.7 (4.98)

#: In chloroform. sh: Shoulder.

ca. 250~256 nm. From these electronic spectral data, it was also certified that each of the **$(C_nS)_6$PcCu-C_{60}** (**1a–1c**) derivatives bears a fullerene moiety.

Thus, we confirmed from MALDI-TOF mass spectra and the UV-vis spectra that all the target Pc-C_{60} dyads, **$(C_nS)_6$PcCu-C_{60}** (**1a–1c**), could be successfully synthesized.

Phase transition behavior

Phase transition behavior and X-ray data of the precursors (**4a–4c**, **5a–5c**) and the Pc-C_{60} dyads (**1a–1c**) are summarized in Tables 4 and 5, respectively. The phase transition behaviors were established by using a polarizing microscope, a differential scanning calorimeter, and a temperature-dependent small angle X-ray diffractometer.

As can be seen from Table 4, each of the derivatives showed only one mesophase, hexagonal ordered columnar (Col_{ho}) phase. Very interestingly, the clearing point (cp) uniformly decreased with the substituents changing as **OH** (**4**) → **OFBA** (**5**) → **C_{60}** (**1**): **4a** (-35 °C) **5a** (-85°C) **1a**; **4b** (-20 °C) **5b** (-98 °C) **1b**; **4c** (-12 °C) **5c** (-84 °C). Especially, it should be notable that when OFBA → C_{60}, the cp drastically decreased by 84 °C~98 °C. This may be attributed to the big steric hindrance of spherical fullerenes weakening the intermolecular force between phthalocyanine disks in the column.

Very interestingly, each of the **$(C_nS)_6$PcCu-C_{60}** (**1a–4c**) dyads shows homeotropic alignment, although none of the corresponding Pc precursors of **$(C_nS)_6$PcCu-OH** (**4a–4c**) and **$(C_nS)_6$PcCu-OFBA** (**5a–5c**) does not show homeotropic alignment. When the Pc-C_{60} dyad (**1a–1c**) between two glass plates was heated up over their cp and then the isotropic liquid was cooled down under the cp, it showed perfect homeotropic alignment. The left part of Fig. 3 shows a photomicrograph of the homeotropically aligned Col_{ho} mesophase of **1a** between cross polarizers at

Table 4. Phase transition temperatures and enthalpy changes

Compound	Phase $\xrightarrow{T/^{\circ}C[\Delta H(kJmol^{-1})]}$ Phase
4a: $(C_{14}S)_6$PcCu-OH	$K_{2v} \xrightarrow{50.0\ [73.0]} Col_{ho} \rightleftharpoons$ I.L.; $K_1 \xrightarrow{15.0\ [44.1]} Col_{ho}$
4b: $(C_{16}S)_6$PcCu-OH	$K \rightleftharpoons Col_{ho} \xrightarrow{288.3\ [6.98]}$ I.L.
4c: $(C_{18}S)_6$PcCu-OH	$K_2 \xrightarrow{57.6\ ^{*2}} Col_{ho} \rightleftharpoons$ I.L.; $K_1 \xrightarrow{37.7\ ^{*1}} Col_{ho}$; *1 + *2 = [101.8]
5a: $(C_{14}S)_6$PcCu-OFBA	$K_{2v} \xrightarrow{37.2\ ^{*1}} K_{3v} \xrightarrow{60.2\ ^{*2}} Col_{ho} \rightleftharpoons$ I.L.; $K_1 \xrightarrow{5.0\ [33.2]} Col_{ho}$; *1 + *2 = [63.6]
5b: $(C_{16}S)_6$PcCu-OFBA	$K \rightleftharpoons Col_{ho} \xrightarrow{268.2\ [6.25]}$ I.L.
5c: $(C_{18}S)_6$PcCu-OFBA	$K_2 \xrightarrow{44.4\ ^{*3}} Col_{ho} \rightleftharpoons$ I.L.; $K_1 \xrightarrow{49.2\ ^{*4}} Col_{ho}$; *3 + *4 = [132.2]
1a: $(C_{14}S)_6$PcCu-C_{60}	$K_2 \xrightarrow{-8.10\ [11.6]} \boxed{Col_{ho}} \rightleftharpoons$ I.L.; $K_{1v} \xrightarrow{-15.6\ [10.1]} \boxed{Col_{ho}}$
1b: $(C_{16}S)_6$PcCu-C_{60}	$K_{2v} \xrightarrow{29.2\ [5.36]} K_3 \xrightarrow{42.1\ [33.8]} \boxed{Col_{ho}} \rightleftharpoons$ I.L.; $K_1 \xrightarrow{23.3\ [28.2]} \boxed{Col_{ho}}$
1c: $(C_{18}S)_6$PcCu-C_{60}	$K_2 \xrightarrow{52.1\ [ca.\ 107]} \boxed{Col_{ho}} \rightleftharpoons$ I.L.; $K_{1v} \xrightarrow{31.5\ [60.6]} \boxed{Col_{ho}}$

Phase nomenclature: K = crystal, Col_{ho} = hexagonal ordered columnar mesophase, Col_{hd} = hexagonal disordered columnar mesophase, I.L. = isotropic liquid, and v = virgin sample. $\boxed{\ }$ = mesophase showing homeotropic alignment for the non-virgin state.

rt. The right part of this figure shows a photomicrograph of the scratched film. As can be seen from the left photomicrograph, the homeotropic alignment gave a completely dark area. On the other hand, as can be seen from the right photomicrograph, the scratched part only gave bright area. Under these photomicrographs in Fig. 3, schematic models of these alignments are illustrated. The scratched parts gave disordered alignment of columns as illustrated in this figure, so that the parts only turn to bright area due to the resulted birefringence.

To date, we have synthesized several kinds of Pc-C_{60} dyads showing perfect homeotropic alignment [19, 28, 30, 35, 36]. Each of them, *e.g.* **$[(C_{12}O)_2PhO]_6$PcCu-C_{60}** [36], was obtained from a corresponding homeotropic alignment-showing parent Pc compound, **$[(C_nO)_2PhO]_8$-PcCu** [31]. In this work, we could synthesized the novel homeotropic alignment-showing Pc-C_{60} dyads, **$(C_nS)_6$PcCu-C_{60}** (**1a–1c**), at the first time, from the non-homeotropic alignment-showing parent Pc compound **$(C_nS)_8$PcCu** [38] and the Pc precursors **$(C_nS)_6$PcCu-OH** (**4a–4c**) and **$(C_nS)_6$PcCu-OFBA** (**5a–5c**). It may be attributed to the strong affinity between fullerene and glass surface. Although the reason is not so clear at the present time, this is very useful guideline for the molecular design to prepare homeotropic alignment-showing discotic liquid crystals. Furthermore, it is noteworthy that the derivative **$(C_{14}S)_6$PcCu-C_{60}** (**1a**) shows perfect homeotropic alignment from rt to 110 °C

Table 5. X-ray data of **4a–4c**, **5a–5c** and **1a–1c**

Compound (mesophase)	Lattice constants/Å	Spacing/Å		Miller indices
		Observed	Calculated	(*h k l*)
4a: ($C_{14}S$)$_6$PcCu-OH	a = 35.9	31.1	31.1	(1 0 0)
(Col_{ho} at 180 °C)	*h* = 3.58	17.7	17.9	(1 1 0)
	Z = 1.1 for ρ = 1.0	15.6	15.5	(2 0 0)
		ca. 4.8	—	#
		3.58	—	(0 0 1)[h]
4b: ($C_{16}S$)$_6$PcCu-OH	a = 36.3	31.5	31.5	(1 0 0)
(Col_{ho} at 180 °C)	*h* = 3.51	18.3	18.2	(1 1 0)
	Z = 1.1 for ρ = 1.0	15.8	15.7	(2 0 0)
		11.9	11.9	(2 1 0)
		ca. 4.8	—	#
		3.51	—	(0 0 1)[h]
4c: ($C_{18}S$)$_6$PcCu-OH	a = 39.4	34.4	34.1	(1 0 0)
(Col_{ho} at 150 °C)	*h* = 3.47	19.2	19.7	(1 1 0)
	Z = 1.1 for ρ = 1.0	17.0	17.0	(2 0 0)
		ca. 4.7	—	#
		3.47	—	(0 0 1)[h]
5a: ($C_{14}S$)$_6$PcCu-OFBA	a = 36.2	31.0	31.0	(1 0 0)
(Col_{ho} at 200 °C)	h = 3.50	17.9	18.1	(1 1 0)
	Z = 1.1 for ρ = 1.0	15.7	15.7	(2 0 0)
		ca. 4.9	—	#
		3.50	—	(0 0 1)[h]
5b: ($C_{16}S$)$_6$PcCu-OFBA	a = 37.8	32.7	32.7	(1 0 0)
(Col_{ho} at 100 °C)	*h* = 3.46	18.8	18.9	(1 1 0)
	Z = 1.1 for ρ = 1.0	16.3	16.4	(2 0 0)
		12.2	12.4	(2 1 0)
		ca. 4.6	—	#
		3.46	—	(0 0 1)[h]
5c: ($C_{18}S$)$_6$PcCu-OFBA	a = 39.7	34.4	34.4	(1 0 0)
(Col_{ho} at 70 °C)	*h* = 3.44	19.6	19.9	(1 1 0)
	Z = 1.1 for ρ = 1.0	17.5	17.2	(2 0 0)
		13.2	13.0	(2 1 0)
		ca. 4.7	—	#
		3.44	—	(0 0 1)[h]
1a: ($C_{14}S$)$_6$PcCu-C_{60}	a = 36.4	75.4	—	H
(Col_{ho} at r.t)	*h* = 3.43	31.5	31.5	(1 0 0)
	Z = 0.8 for ρ = 1.0	18.2	18.2	(1 1 0)
		ca. 4.6	—	#
		3.43	—	(0 0 1)[h]
1b: ($C_{16}S$)$_6$PcCu-C_{60}	a = 36.7	73.9	—	H
(Col_{ho} at 60 °C)	*h* = 3.44	31.7	31.7	(1 0 0)
	Z = 1.3 for ρ = 1.0	18.7	18.4	(1 1 0)
		ca. 4.6	—	#
		3.44	—	(0 0 1)[h]
1c: ($C_{18}S$)$_6$PcCu-C_{60}	a = 39.7	79.6	—	H
(Col_{ho} at 70 °C)	*h* = 3.47	34.4	34.4	(1 0 0)
	Z = 0.9 for ρ = 1.0	19.6	19.9	(1 1 0)
		ca. 4.6	—	#
		3.47	—	(0 0 1)[h]

= Halo of the molten alkyl chain, *h* = Stacking distance between the monomers. H = Helical pitch of the fullerenes. ρ: assumed density (g/cm^3)

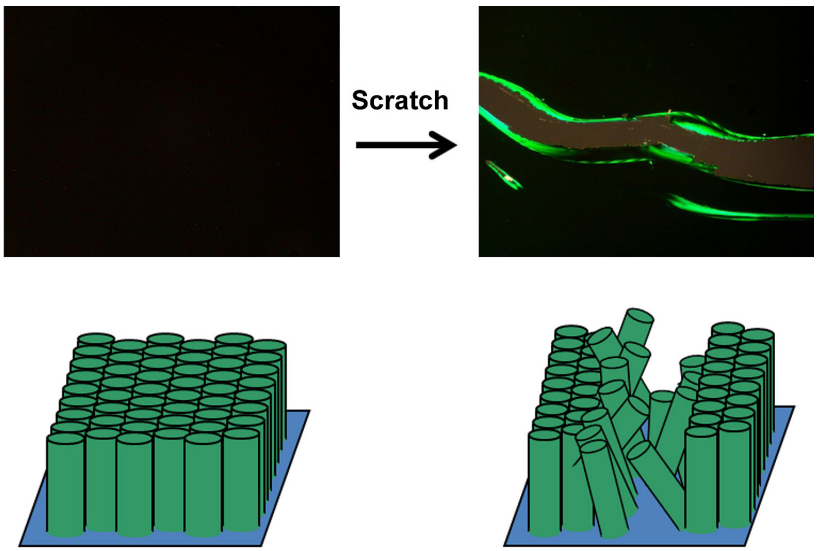

Fig. 3. Photomicrographs of $(C_{14}S)_6PcCu\text{-}C_{60}$ (**1a**) at rt and schematic models of the columnar alignments

not only between two glass plates but also on a glass plate. The homeotropic alignment-showing thin film could be easily obtained only by casting the chloroform solution of **1a** onto a glass plate at rt. It is very favorable for the fabrication of organic thin film solar cells.

Temperature-dependent SAXS study

Figure 4 shows temperature-dependent small angle X-ray diffraction patterns of the Pc precursors **4b**, **5b** and the Pc-C_{60} dyad **1b**. These X-ray diffractions were measured by using a sample packed in a small hole of glass plate as illustrated in Fig. 5a. As can be seen from Fig. 4, each of the Pc precursors, **4b** at 180 °C and **5b** at 100 °C, gave four sharp peaks in the low angle region and two broad peaks in the high angle region, respectively. These four peaks in the low angle region were assigned to the reflections from (100), (110) and (210) planes of a 2D hexagonal lattice (Table 5). On the other hand, in the high angle region the big broad peak corresponds to the molten alkylthio chains and the small broad peak was assigned to the reflection from (001) plane corresponding to the stacking distance between the Pc disks in a column. Hence, this mesophase was identified as a hexagonal ordered columnar (Col_{ho}) phase.

As can be seen from the X-ray diffraction pattern of the dyad **1b** at 60 °C gave the reflections from (100), (110) and (001) in a Col_{ho} mesophase similarly to the Pc precursors **4b** and **5b**. However, it gave an additional large reflection peak around $2\theta = 1^{o}$, which is denoted as Peak H hereafter. This Peak H could not be observed for the Col_{ho} mesophases of the Pc precursors **4b** and **5b**, as can be seen from Fig. 4. Moreover, it could not be assigned to any reflections from all the 2D lattices of liquid crystalline phases known until now.

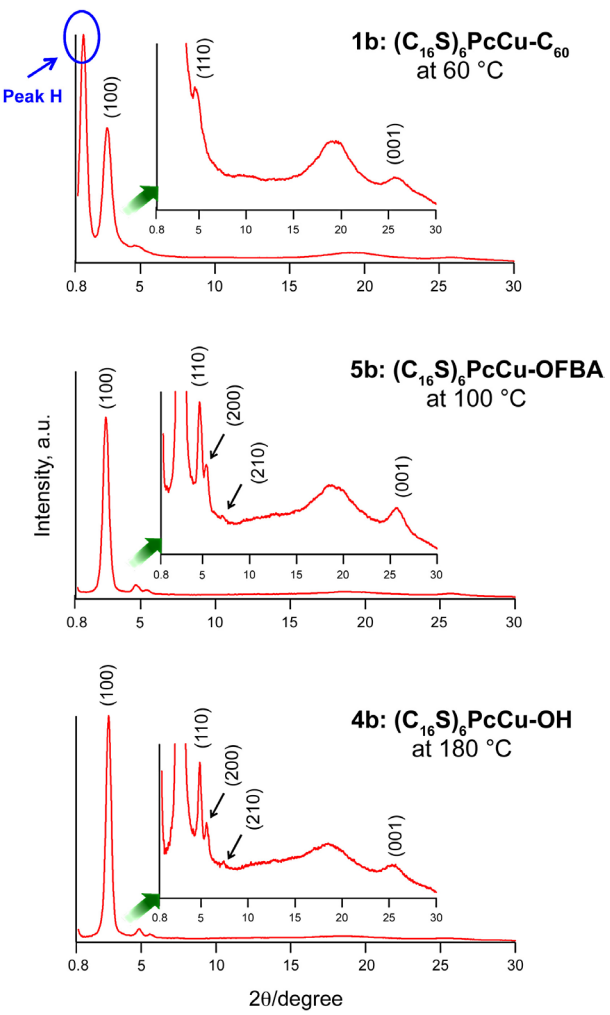

Fig. 4. Small angle X-ray diffraction patterns of $(C_{16}S)_6PcCu\text{-}OH$, $(C_{16}S)_6PcCu\text{-}OFBA$ and $(C_{16}S)_6PcCu\text{-}C_{60}$

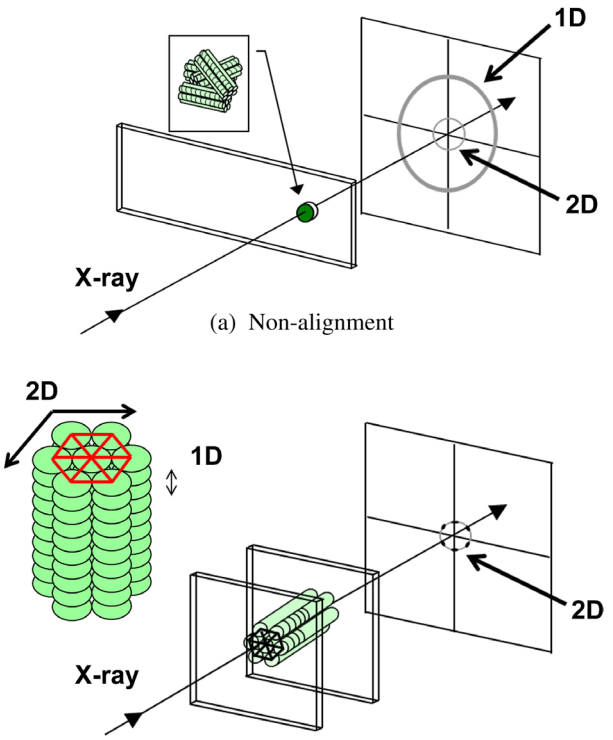

Fig. 5. Illustration of X-ray photograph of (a) non-alignment and (b) homeotropic alignment of ordered columns between two glass plates

Recently, we also observed this additional peak in the same small angle region for the previously reported Pc-C_{60} dyad, **[$(C_{12}O)_2$PhO]$_6$PcCu-C_{60}**. It was revealed from the precise X-ray structure analysis that this peak is originated from a helical structure of fullerene moieties [36]. In order to certify that Peak H of the present Pc-C_{60} dyads, (C_nS)$_6$PcCu-C_{60} (**1a–1c**), may be also originated from the helical structure of fullerene moieties, we have carried out X-ray diffraction measurements using our previously developed methods [36].

When a sample is packed in a hole of glass plate as illustrated in Fig. 5a, both reflection peaks due to the columnar packing in the 2D lattice (XY-axes) direction and reflection peaks due the stacking in the 1D lattice (Z-axis) direction can be observed, because the domains are formed in all directions. On the other hand, when a sample is cleared over cp and then cooled down below cp between two cover glass plates to form perfect homeotropic alignment as illustrated in Fig. 5b, reflection peaks from the 2D lattice only appear but reflection peaks from the 1D lattice disappear, because all the columns align in one direction perpendicular to the glass plates. As already mentioned above, the present Pc-C_{60} dyads, **(C_nS)$_6$PcCu-C_{60}** (**1a–1c**), show perfect homeotropic alignment between two glass plates, which was revealed by polarizing microscopic observations. Therefore, if Peak H would be along the

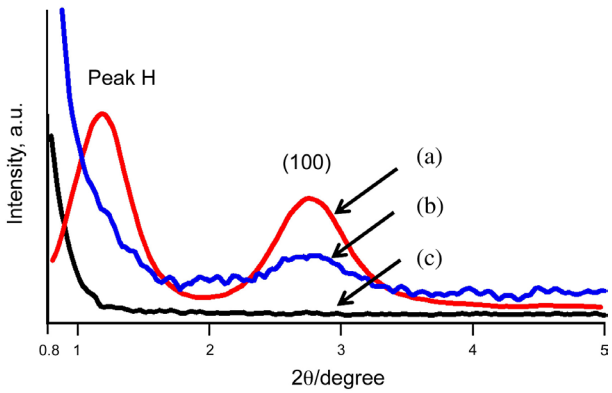

Fig. 6. Small angle X-ray diffraction patterns of the Col_{ho} mesophase in **($C_{16}S)_6$PcCu-C_{60}** (**1b**): (a) non-homeotropically aligned sample at 60 °C, (b) homeotropically aligned sample between two glass plates at 120 °C and (c) only two soda-lime glass plates at 120 °C

1D lattice (Z-axis) direction, it should disappear in the X-ray diffraction pattern for the homeotropically aligned sample, as illustrated in Fig. 5b.

Figures 6a and 6b show the small angle X-ray diffraction patterns of the Col_{ho} mesophase in the Pc-C_{60} dyad, **($C_{16}S)_6$PcCu-C_{60}** (**1b**), for the samples prepared by using two methods illustrated in Figs 5a and 5b, respectively. As can be seen from Fig. 6a, the non-homeotropically aligned sample gave both (100) reflection peak and Peak H. On the other hand, as can be seen from Fig. 6b, the homeotropically-aligned sample gave clearly the (100) peak from the 2D lattice in XY-axes direction, but Peak H completely disappeared. Therefore, Peak H should be a periodicity in Z-axis direction. Since the spacing of this Peak H is 75.4 Å, it cannot be a stacking distance between the Pc disks in the columnar structure. This peak appears only for the Pc-C_{60} dyad (**1**), but it does not appear for the Pc precursors, **4** and **5**. Hence, it can be attributed to the stacking distance of fullerene moieties. The stacking distance of the Pc disks in column is 3.43 Å, so that twenty-two fullerenes may stack, as can be calculated from an equation of 75.4 Å/3.43 Å = 22. Since the diameter of a fullerene is 10 Å, twenty-two fullerenes cannot linearly stack in 75.4 Å, which is much shorter than 220 Å (= 10 Å × 22). Therefore, the fullerene moieties should stack helically in Z-axis direction. If the fullerene moieties would stack randomly in Z-axis direction, the periodicity at 75.4 Å would not appear. Accordingly, we can conclude that the present **(C_nS)$_6$PcCu-C_{60}** (**1a–1c**) dyads also show perfect homeotropic alignment forming spiranthes-like [37] supramolecular structure, similarly to the previous **[(C_nO)$_2$PhO]$_6$PcCu-C_{60}** dyads illustrated in Fig. 1b. This supramolecular structure is compatible with 1D nano-array [5] illustrated in Fig. 1a. Therefore, the present spiranthes-like supramolecular structure of **1a–1c** may be more favorable for the application to organic thin film solar cells to raise their conversion efficiencies [45],

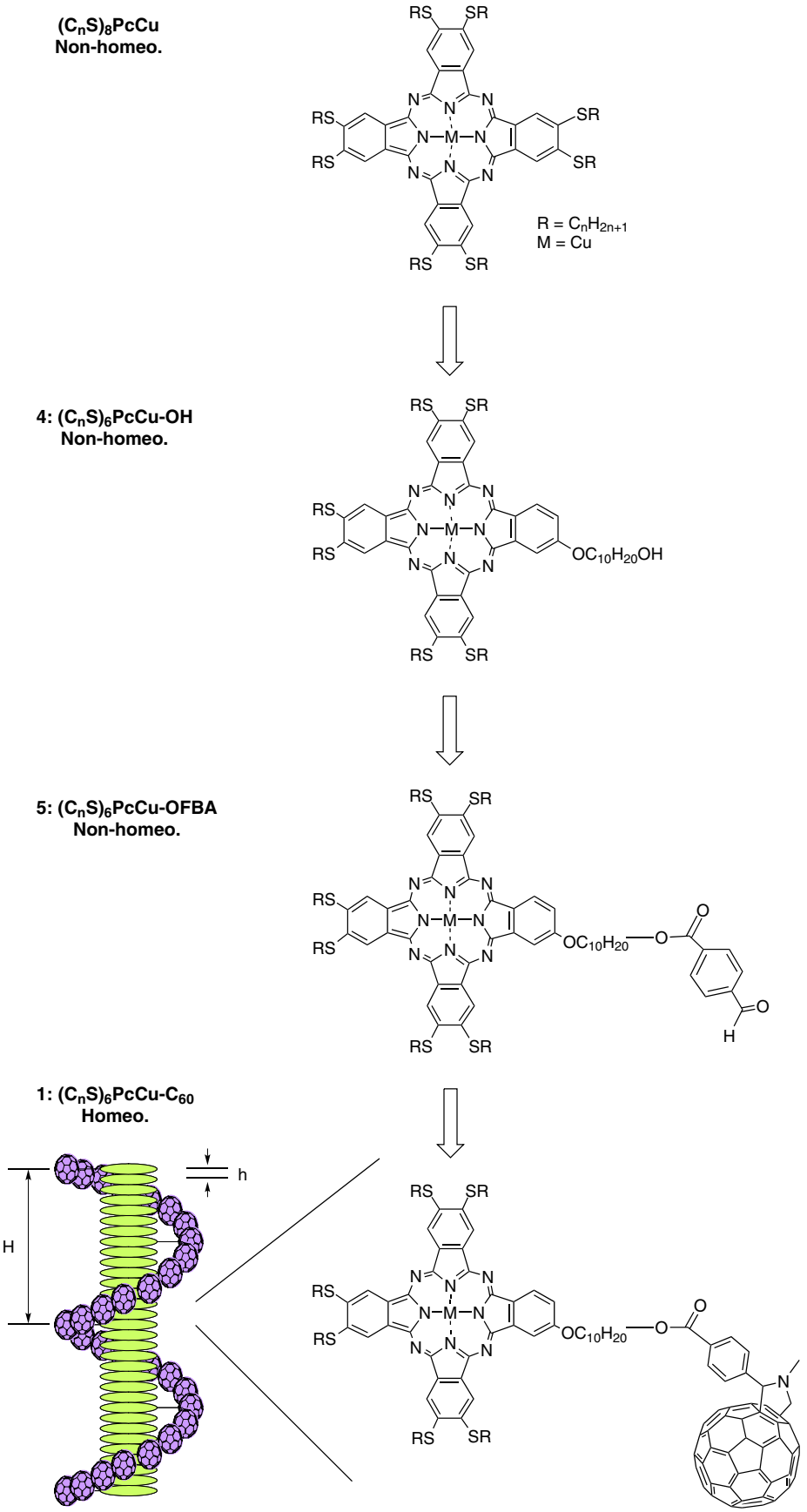

Fig. 7. Novel **$(C_nS)_6$PcCu-C_{60}** dyads (**1a–1c**) showing homeotropic alignment with spiranthes-like supramolecular structure obtained from their non-homeotropic parent **$(C_nS)_8$PcCu** compounds and precursors **$(C_nS)_6$PcCu-OH** (**4**) and **$(C_nS)_6$PcCu-OFBA** (**5**)

because the present dyads **1a–1c** can be more easily synthesized than the previous **[$(C_nO)_2$PhO]$_6$PcCu-C_{60}** dyads.

CONCLUSION

We have synthesized novel liquid crystalline donor–acceptor dyads, **$(C_nS)_6$PcCu-C_{60}** (n = 14, 16, 18: **1a–1c**), connected alkylthio-substituted PcCu and fullerene. The mesomorphic properties and alignment behavior have been established for the Pc-C_{60} dyads (**1a–1c**) together with their Pc precursors, **$(C_nS)_6$PcCu-OH** (**4a–4c**) and **$(C_nS)_6$PcCu-OFBA** (**5a–5c**). Each of the derivatives, **4**, **5** and **1**, shows only one mesophase, Col_{ho}. As summarized in Fig. 7, neither the parent Pc compounds **$(C_nS)_8$PcCu** (**1a–1c**) nor the Pc precursors of **$(C_nS)_6$PcCu-OH** (**4a–4c**) and **$(C_nS)_6$PcCu-OFBA** (**5a–5c**) show homeotropic alignment, whereas the Pc-C_{60} dyads, **$(C_nS)_6$PcCu-C_{60}** (**1a–1c**), show perfect homeotropic alignment between two glass plates for the Col_{ho} mesophase. It may be attributed to the strong affinity between fullerene and glass surface. Although the reason is not so clear at the present time, this is very useful guideline for the molecular design to prepare homeotropic alignment-showing discotic liquid crystals. Very interestingly, in the Col_{ho} mesophase the Pc-C_{60} dyads **1a–1c** form "Spiranthes-like" supramolecular structure in which the Pc disks stack face-to-face to form columns and the fullerene moieties helically stack around the columns. This supramolecular structure is compatible with the 1D nano-array structure proposed by Yoshikawa *et al.*, so that the present Pc-C_{60} dyads (**1a–1c**) are very favorable for the application to organic thin film solar cells to raise the conversion efficiency.

Acknowledgements

This work is partially supported by Grant-in-Aid for Green Innovation Research in 2013 from Shinshu University, Japan.

Supporting information

Figures S1–S4 are given in the supplementary material. This material is available free of charge *via* the Internet at http://www.worldscinet.com/jpp/jpp.shtml.

REFERENCES

1. Li ZG, Zhao XY, Lu X, Gao ZQ, Mi BX and Huang W. *Sci. China: Chem.* 2012; **55**: 553–578.
2. Ozaki M. *Kagaku Kogyo* 2011; **62**: 62–69.
3. Zhao XY, Mi BX, Gao ZQ and Huang W. *Sci. China: Phys. Mech. Astron.* 2011; **54**: 375–387.
4. Hiramoto M. *J. Vac. Soc. Jpn* (*Nippon Shinku Kyokai*) 2010; **53**: 13–18.
5. Yoshikawa S. *Supra-hierarchical Nano-structured Organic Thin Film Solar Cells*, JST-DFG Joint WS http://www.jst.go.jp/sicp/ws2009_ge3rd/abstract/20.pdf.
6. Kim JY and Bard AJ. *Chem. Phys. Lett.* 2004; **383**: 11–15.
7. Nishizawa T, Tajima K and Hashimoto K. *J. Mater. Chem.* 2007; **17**: 2440–2445.
8. Roland T, Ramirez GH, Léonard J, Méry S and Haacke S. *J. Phys.: Conference Series* 2011; **276**: 012006(1–6).
9. Lincker F, Heinrich B, Bettignies R, Rannou P, Pecaut J, Grevin B, Pron A, Donnio B and Demadrille R. *J. Mater. Chem.* 2011; **21**: 5238–5247.
10. Barrau S, Heiser T, Richard F, Brochon C, Ngov C, van de Wetering K, Hadziioannou G, Anokhin DV and Ivanov DA. *Macromolecules* 2008; **41**: 2701–2710.
11. Kim DH, Lee BL, Moon H, Kang HM, Jeong EJ, Park JI, Han KM, Lee S, Yoo BW, Koo BW, Kim JY, Lee YH, Cho K, Becerril HA and Bao Z. *J. Am. Chem. Soc.* 2009; **131**: 6124–6132.
12. Liang TC, Chiang IH, Yang PJ, Kekuda D, Chu CW and Lin HC. *J. Poly. Sci.: Part A Poly. Chem.* 2009; **47**: 5998–6013.
13. Sommer M, Huettner S and Thelakkat M. *J. Mater. Chem.* 2010; **20**: 10788–10797.
14. Yao K, Chen Y, Chen L, Li F, Li X, Ren X, Wang H and Liu T. *Macromolecules* 2011; **44**: 2698–2706.
15. Yasuda T, Yonezawa K, Ito M, Kamioka H, Han L and Moritomo Y. *J. Photopolym. Sci. Technol.* 2012; **25**: 271–276.
16. Han Y, Chen L and Chen Y. *J. Poly. Sci. Poly. Chem.* 2012; published online: DOI: 10.1002/pola.26394.
17. Li F, Chen W and Chen Y. *J. Mater. Chem.* 2012; **22**: 6259–6266.
18. Bushby JR, Hamley IW, Liu Q, Lozman OR and Lydon EJ. *J. Mater. Chem.* 2005; **15**: 4429–4434.
19. Uchida S, Kude Y, Nishikitani Y and Ota (= Ohta) K. *Jpn. Kokai Tokkyo Koho.* JP 2008214227(A)-2008-09-18 (priority number: JP2007060604; submission date: 2007-03-09).
20. Zhou X, Kang SW, Kumar S, Kulkarni RR, Cheng SZD and Li Q. *Chem. Mater*. 2011; **20**: 3551–3553.
21. de la Escosura A, Martınez-Dıaz MV, Barbera J and Torres T. *J. Org. Chem*. 2008; **73**: 1475–1480.
22. Tashiro K and Aida T. *J. Am. Chem. Soc.* 2008; **130**: 13812–13813.
23. Geerts YH, Debever O, Amato C and Sergeyev S. *Beilstein J. Org. Chem.* 2009; **5**: 1–9.
24. Thiebaut O, Bock H and Grelet E. *J. Am. Chem. Soc.* 2010; **132**: 6886–6887.
25. Hayashi H, Nihashi W, Umeyama T, Matano Y, Seki S, Shimizu Y and Imahori H. *J. Am. Chem. Soc.* 2011; **133**: 10736–10739.
26. Bagui M, Dutta T, Chakraborty S, Melinger JS, Zhong H, Keightley A and Peng Z. *J. Phys. Chem. A* 2011; **115**: 1579–1592.

27. Haverkate LA, Zbiri M, Johnson MR, Deme B, de Groot HJM, Lefeber F, Kotlewski A, Picken SJ, Mulder FM and Kearley GJ. *J. Phys. Chem. B* 2012; **116**: 13098–13105.
28. Ota (= Ohta) K. *Jpn. Kokai Tokkyo Koho* JP201-1132180(A)-2011-07-07 (priority number: JP2009-0293501; submission date: 2009-12-24).
29. Ince M, Martinez-Diaz MV, Barbera J and Torres T. *J. Mater. Chem.* 2011; **21**: 1531–1536.
30. Kamei T, Kato T, Itoh E and Ohta K. *J. Porphyrins Phthalocyanines* 2012; **16**: 1261–1275.
31. Hatsusaka K, Ohta K, Yamamoto I and Shirai H. *J. Mater. Chem.* 2001; **11**: 423–433.
32. Hatsusaka K, Kimura M and Ohta K. *Bull. Chem. Soc., Jpn.* 2003; **76**: 781–787.
33. Mukai H, Hatsusaka K and Ohta K. *J. Porphyrins Phthalocyanines* 2007; **11**: 846–856.
34. Ariyoshi M, Sugibayashi-Kajita M, Suzuki-Ichihara A, Kato T, Kamei T, Itoh E and Ohta K. *J. Porphyrins Phthalocyanines* 2012; **16**: 1114–1123.
35. Shimizu M, Tauchi L, Nakagaki T, Ishikawa A, Itoh E and Ohta K. *J. Porphyrins Phthalocyanines* 2013; **17**: 264–282.
36. Tauchi L, Nakagaki T, Shimizu M, Itoh E, Yasutake M and Ohta K. *J. Porphyrins Phthalocyanines* 2013; **17**: 1080–1093.
37. http://en.wikipedia.org/wiki/Spiranthes.
38. Ban K, Nishizawa K, Ohta K and Shirai H. *J. Mater. Chem*. 2000; **10**: 1083–1090.
39. Serin S and Karabörk M. *Synthesis and Reactivity in Inorganic and Metal-Organic Chemistry*, 2002; **32**: 1635–1647.
40. Wöhrle D, Eskes M, Shigehara K and Yamada A. *Synthesis* 1993; 194–196.
41. Neises B and Steglish W. *Angew. Chem. Int. Ed.* 1978; **17**: 522–524.
42. Maggini M, Scorrano G and Prato M. *J. Am. Chem. Soc.* 1993; **115**: 9798–9799.
43. van der Pol JF, Neeleman E, van Miltenburg JC, Zwikker JW, Nolte RJM and Drenth W. *Macromolecules* 1990; **23**: 155–162.
44. Sastre A, Gouloumis A, Vazquez P, Torres T, Doan V, Schwartz BJ, Wudl F, Euhegoyen L and Rivera J. *Org. Lett.* 1999; **1**: 1807–1810.
45. Osaka I, Saito M, Koganezawa T and Takimiya K. *Adv. Mater.* Article first published online: 8 oct. 2013, DOI: 10.1002/adma.201303059.